JOM, Vol. 69, No. 3, 2017
DOI: 10.1007/s11837-017-2264-3

Strategy for Texture Management in Metals Additive Manufacturing

M.M. KIRKA,[1,2,3] Y. LEE,[1,2] D.A. GREELEY,[1] A. OKELLO,[1,2] M.J. GOIN,[1] M.T. PEARCE,[1] and R.R. DEHOFF[1,2]

1.—Manufacturing Demonstration Facility, Oak Ridge National Laboratory, Knoxville, TN, USA. 2.— Materials Science and Technology Division, Oak Ridge National Laboratory, Oak Ridge, TN, USA. 3.—e-mail: kirkamm@ornl.gov

Additive manufacturing (AM) technologies have long been recognized for their ability to fabricate complex geometric components directly from models conceptualized through computers, allowing for complicated designs and assemblies to be fabricated at lower costs, with shorter time to market, and improved function. Lacking behind the design complexity aspect is the ability to fully exploit AM processes for control over texture within AM components. Currently, standard heat-fill strategies utilized in AM processes result in largely columnar grain structures. Proposed in this work is a point heat source fill for the electron beam melting (EBM) process through which the texture in AM materials can be controlled. Through this point heat source strategy, the ability to form either columnar or equiaxed grain structures upon solidification through changes in the process parameters associated with the point heat source fill is demonstrated for the nickel-base superalloy, Inconel 718. Mechanically, the material is demonstrated to exhibit either anisotropic properties for the columnar-grained material fabricated through using the standard raster scan of the EBM process or isotropic properties for the equiaxed material fabricated using the point heat source fill.

INTRODUCTION

Additive manufacturing (AM) has become well known for its ability to fabricate geometries of unlimited complexity not possible by traditional means[1]. However, due to the high solidification velocities combined with the high thermal gradients present in the solidifying melt pool of AM metals, a highly textured structure forms. In instances where the material exhibits crystallographic anisotropy, the resulting columnar-grained material exhibits anisotropic mechanical properties similar to directionally solidified nickel-base (Ni-base) superalloys.[2] As a result, having the means of controlling texture formation in AM materials in a manner to allow either equiaxed or columnar grains as needed based upon the application of the material is beneficial.

While not considered AM by current standards, the desire for texture control in AM processes can be traced back to the work of Gäumann et al.[3] in which minimizing the formation of stray grains in the repair of single crystal airfoils was required. Their work can further be traced to that of Babu et al.[4] in their efforts to weld single-crystal Ni-base superalloys. Within the context of AM, Dinda et al.[5] were the first to report on the ability to steer the growth direction of grains through changing the direction of the laser heat source. Later, Dehoff et al.[6] demonstrated the premise of texture control within AM materials in a site-specific manner in the electron beam melting (EBM) process, through manipulation of the thermal conditions within the melt pool in the different regions, although not in a perfect manner. Recently, Helmer et al.[7,8] have shown the ability to influence the grain structure in the EBM process for

(Published online January 31, 2017)

Inconel 718 through changing the parameters associated with the standard raster scan strategy utilized by the process. However, based on the black box algorithm of the EBM process, applying texture control over generic cross-sections within bulk structures in a controlled manner is extremely challenging.

The ability to control texture within metals fabricated by AM provides a similar capability to influence the mechanical performance of structures similar to those capabilities found in castings.[9] Through this work, a point heat source melt strategy is proposed and compared to the traditional raster (snake) scan strategy currently utilized for filling the melt area in the EBM process. To demonstrate the ability to control texture within EBM-processed material, the Ni-base superalloy Inconel 718 is utilized due to the favorable position of the transition between columnar and equiaxed grains in relation to the EBM processing space. The tensile properties at both room temperature and 650°C for the material fabricated through the traditional raster scan strategy and proposed point heat source fill is demonstrated. Ultimately, through this proposed heat source fill strategy, the ability to transition between columnar and equiaxed grain structures is demonstrated on the Ni-base superalloy Inconel 718.

MATERIALS AND METHODS

Electron Beam Melting Process

For fabricating the samples considered in this study, the AM Arcam EBM process was utilized. An Arcam S12 EBM system running EBM Control V4.1.89 process software was used for the builds reported here. The Arcam S12 used is modified with an enhanced electron gun making the system identical to that of an Arcam A1 system. For all builds, 304 stainless steel (150 × 150 × 10 mm) was used as the start plate material. All builds were started once a temperature of 1100°C was achieved and held for 30 min to sinter the powder beneath the start plate. Throughout the build process, a chamber vacuum level of 2×10^{-3} mBar was maintained. For all builds, a layer thickness of 50 μm was used. The accelerating voltage of the electron gun was set to 60 kV. Sections "Point Heat Source Fill" and "Mechanical Test Sample Build" present the specifics of the individual build layouts and process parameters utilized in the builds.

Feedstock Material

The Inconel 718 feedstock powder (Nominal chemistry listed in Table I) was manufactured by AP&C (Quebec, Canada) with a particle size range of 40–120 μm using the plasma wire atomization process.

Raster Scan Strategy

The standard raster heat source scan strategy fill utilized in the Arcam EBM process is illustrated in Fig. 1. The volumetric energy density associated with the raster scan of a given material point can be estimated by the following equation:

$$E_v = \frac{i(\mathrm{SF})V}{v(\mathrm{SF})h_s z} \tag{1}$$

where V is the accelerating voltage of the electron beam, h_s the hatch spacing, z the layer thickness, scan velocity (v(SF)), and i(SF) the beam current, where both are variables dependent on the speed function (SF) and line scan length. Based on the speed function construction, the beam speed and power are inherently linked to the 2D area geometry of the melt. The basis for this approach is that the melt pool is maintained at a constant cross-section size no matter the length of the line scan for a given speed function.[10] To combat the potential influences of uneven current and speed across a cross-section, the raster scan has the ability to undergo an increasing degree of rotation around the z axis with every increasing layer, as shown in Fig. 1, to smooth out the volumetric energy input.

Point Heat Source Fill

Depicted in Fig. 2 is the point heat source fill designed to give control over the imparted energy density at a given location. In the point heat source fill, the controlling process parameters are the beam current (i_b), the beam spot on time (t_{on}), spacing between neighboring points (l_t), and point skip (l_s) which is equivalent to 10 point spaces. The energy density associated with a spot heat source in the EBM process is given by

$$E_v = \frac{i_b t_{on} V}{z} \tag{2}$$

where the variables retain their previous definitions. The fill occurs in the following fashion assuming a rectangular area:

Table I. Nominal chemical compositions of the Inconel 718 powder used in this work given in weight percent

Cr	Fe	Nb	Mo	Ti	Cu	Al	C	Ni
18.5	18.5	5	3	1	0.15	0.5	0.05	Bal

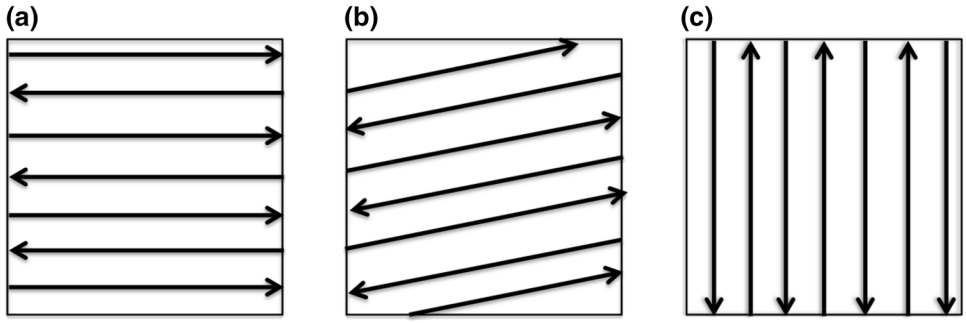

Fig. 1. Raster scan strategy utilized as default by the electron beam heat source depicting an exaggerated rotation of the scan pattern within the build plane for (a) layer n, (b) layer n+1, (c) layer n+2.

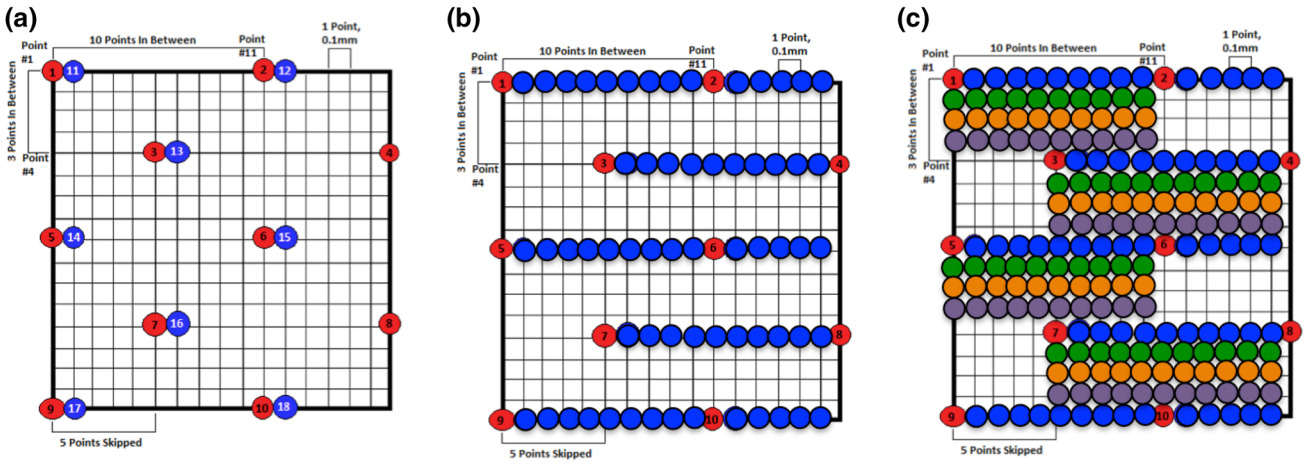

Fig. 2. Exploded view of the point heat source fill detailing the fill of points for (a) the first and second points in each row set, (b) the fill of the first row set, (c) fill of subsequent rows.

1. Row_1 The fill begins in the upper left-hand corner indicated by the point labeled 1 in Fig. 2a where the fist pulse is applied. Following t_{on}, the point heat source is moved a horizontal distance (l_s) equivalent to the spacing of 10 points before the beam pulses again (Point 2). This point skip is repeated until the end of the row is reached.
2. Row_2 At the end of the first row (Point 2 in Fig. 2a), the point heat source is moved vertically down by five rows and horizontally over a distance equivalent to the half the spacing of the initial point skip before pulsing at Point 3 in Fig. 2a. Afterward, the beam repeats the 10-point skip and continues to pulse until the end of the row.
3. Row_3 At the end of the second row (Point 4 in Fig. 2a), the point heat source is moved vertically down by four rows and shifted back to the starting x-coordinate of the first point in the first row. The pulsing sequence described in steps 1 and 2 repeats until the bottom of the area is reached (Point 10).
4. *Row Fill* Once the beam has hit the initial points (Identified by red dots in Fig. 2a), the beam begins to repeat the sequence described in steps 1 through 3 starting with Point 11 in Fig. 2a but offset by a distance of l_t from the first series of points. Upon reaching the bottom of the area to be filled, the beam will continue to return to the first row and continue to shift a distance of l_t before beginning to pulse the beam again. This occurs for a total of 10 times and is illustrated in Fig. 2b.
5. *Area Fill* Once the first set of rows has been filled, the row fill process continues to repeat until the three rows initially skipped (green, orange, and purple in Fig. 2c) are filled using the sequence as described in items 1–4.

To experimentally understand the influence of the parameter space on the resultant texture, arrays of 16 cubes 20 × 20 × 20 mm in size were fabricated by varying both the beam on time and beam current to influence the imparted energy density in the parts. Table II lists the process parameters.

Mechanical Test Sample Build

To characterize the bulk-scale mechanical properties of the differently textured materials fabricated by the standard raster fill and point heat source fill, the build layout shown in Fig. 3a was used with the front of one of the completed builds shown in Fig. 3b. This layout comprised samples in the form of sticks (15 × 15 × 100 mm) and blocks (100 × 100 × 15 mm). The parts were evenly split between the two heat source fills.

For the standard raster scan melt, the process parameters utilized are listed in Table III. In the case of the point heat source fill, the process parameters were a variation (Table IV) of those identified in cube 16 from the parameter space array described previously. The change in parameters was necessary so as not to overheat the reduced cross-sectional melt area of the mechanical test specimen sticks.

Table II. Point heat source fill process parameters explored in this study

Cube number	Current (mA)	Spot time (ms)	Energy density (J/mm^3)
1	5	0.05	15
2		0.075	22.5
3		0.1	30
4		0.25	75
5	10	0.05	30
6		0.075	45
7		0.1	60
8		0.25	150
9	15	0.05	45
10		0.075	67.5
11		0.1	90
12		0.25	225
13	20	0.05	60
14		0.075	90
15		0.1	120
16		0.25	300

To understand build-to-build variation, two builds using identical processing parameters were fabricated. The average build time for this layout was 73 h. In all cases, the builds started at a temperature of 1000°C and completed with a base thermocouple measurement in the 930–945°C range.

Material Post-processing

HIP was conducted using a Quintus QIH-9 equipped with uniform rapid cooling with cooling rates up to 42°C per minute. The material was HIP'd at a temperature of 1200°C and pressure of 120 MPa for a total time of 240 min. Subsequently, solutioning and aging were conducted in a vacuum furnace at the following conditions: solutioning at 1066°C for 60 min, followed by a double aging at 760°C for 10 h, and subsequent cool-down and aging at 650°C for 10 h.

Mechanical Testing

Tensile testing was preformed by Met Cut (Cincinnati, OH, USA) Instron 4505 (electro-mechanical test frame) with MTS Testworks 4 controller, MTS 632.53E−11 (25.4 mm gage length) extensometer. All tensile experiments were conducted according to the applicable ASTM standards.[11,12] From each of the builds, three vertical sticks of the standard raster fill and point heat source fill for a total of six of each heat source fill were tested along the build direction (longitudinal direction). From the blocks, two transverse specimens were taken from each and tested in tension. The remaining specimens from the builds were reserved for low-cycle fatigue and creep testing that will be discussed in a forthcoming work.

Metallogrpahic Preparation and Analysis

After fabrication samples were metallographically prepared using an Allied high-speed cut-off wheel. After sectioning, the samples were successively ground with SiC paper and diamond suspensions before being given a final 0.04-μm colloidal silica finish for texture analysis. The texture of the

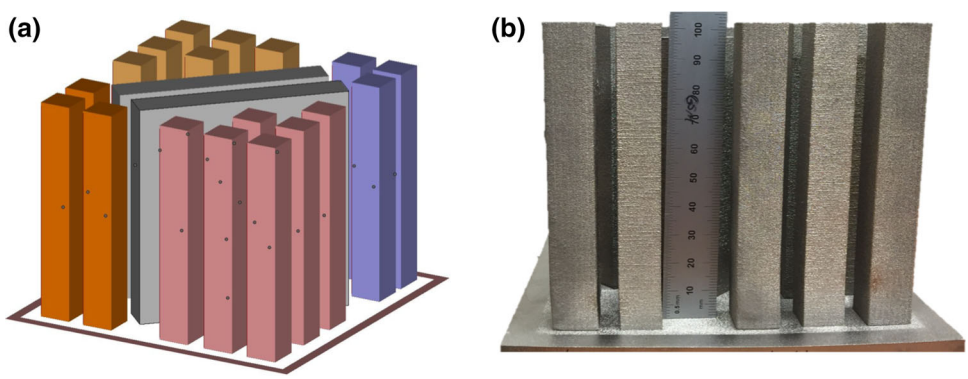

Fig. 3. Build layout used for the fabrication of mechanical test specimen blanks in this study: (a) CAD model, (b) front view of completed EBM build.

samples was studied using a JEOL 6500 field emission scanning electron microscope equipped with a EDAX Hikari EBSD camera. Fracture surfaces of the tensile specimens were imaged using a Keyence VHX-600E digital microscope.

RESULTS AND DISCUSSION

Point Heat Source Fill Microstructures

Figure 4a–c shows the grain orientation maps parallel to the build direction associated with cubes 12, 15, and 16 from the cubic array that explores the point heat source fill parameter space. In this instance, the grain orientation maps are arranged with energy density increasing fromleft to right (120–300 J/mm^3). With increasing energy density, the grain structure transitions from columnar grains oriented parallel to the build direction to a mixture of oriented columnar- and fine-grained structure, to an equiaxed one with the highest energy input. In the case of the dual columnar-grain-sized microstructure, the grain sizes are separated with a horizontal spacing of approximately 0.8–1.5 mm, which is on the same scale as the point skip distance (l_s) used in the point fill pattern.

Table III. Process parameters used for fabricating parts with the standard raster scan fill approach

Speed function	63
Focus offset	7 mA
Hatch spacing	0.125 mm
Preheat current	40 mA

Table IV. Process parameters used for fabricating parts through the point heat source fill approach

Beam current	20 mA
Focus offset	5 mA
Spot time	1.0 ms
Point spacing	0.1 mm
Preheat current	40 mA

Utilizing the finite volume (FVM) code TRUCHAS (developed by Los Alamos National Laboratory), the mechanism through which either columnar or equiaxed grains develop within the melt pool of the point heat source fill strategy is suggested. As the computational intensity associated with modeling a full layer of 40,000 beam pulses is not feasible, a simplified simulation was performed for a set of 10 neighboring spots in a string to provide analytical information on the melt pool shape. In these simulations, the beam is assumed to be 400 μm in diameter with the background temperature being 1000°C.

Figure 5a–c shows the simulated top surfaces of the melt pools for a series of 10 neighboring points corresponding to cubes 15, 12, and 16 at their largest size prior to collapsing during solidification. Due to computational intensity, the entire sequence of points could not be feasibly simulated as a result, the findings are an inference. The finite volume results indicate that an elliptical melt pool forms at the lower energy density of 120 J/mm^3 that is roughly contained within the confines of the first row of points and surrounding unmelted areas, whereas, with increasing energy density, the initial melt pools are theoretical large enough in size and the beating frequency of the beam is fast enough to maintain each of the melt pools, such that melt pools occurring on successive rows are allowed to merge into one another to turn the entire area molten. In the instance of the intermediate energy density (225 J/mm^3), there is not sufficient overlap of the melt pools to cause complete breakdown of the columnar structure and results in the periodic columnar structure with spacing on the order of the point skip spacing l_s.

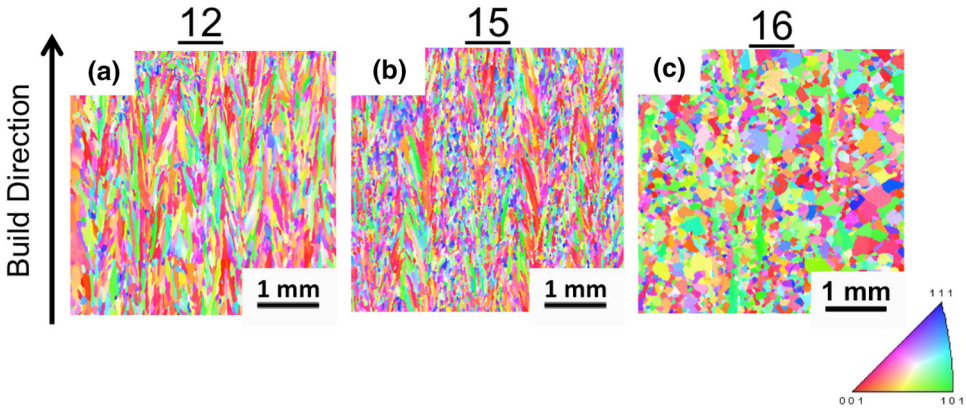

Fig. 4. Grain orientation maps depicting the effect of energy density on the texture of the as-fabricated material parallel to the build direction: (a) cube 15 with $E_v = 120$ J/mm^3, (b) cube 12 $E_v = 225$ J/mm^3, (c) cube 16 $E_v = 300$ J/mm^3.

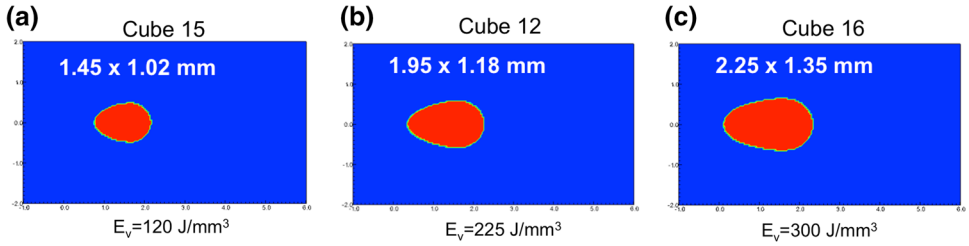

Fig. 5. Simulated melt pool shapes and sizes for 10 neighboring spots for (a) cube 15, (b) cube 12, (c) cube 16.

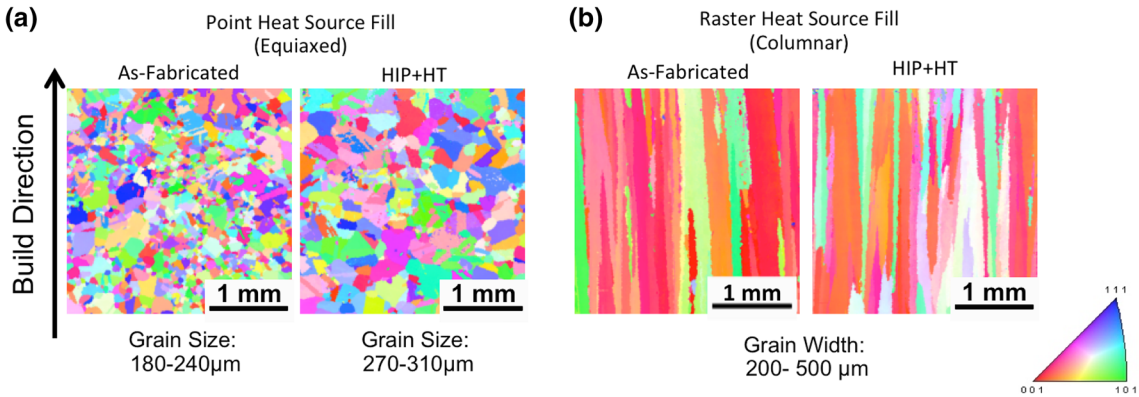

Fig. 6. EBSD grain orientation maps before and after post-processing for (a) material fabricated through the point heat source fill indicating a random texture, (b) columnar grained material fabricated through the standard raster scan strategy.

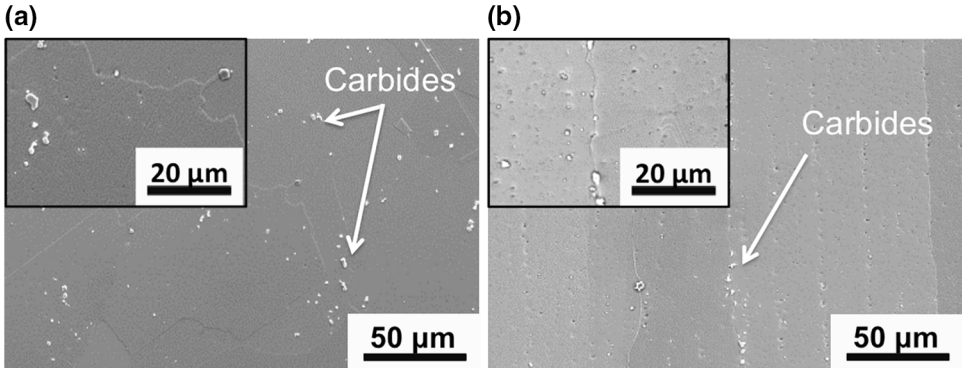

Fig. 7. Representative secondary electron SEM images depicting the location of carbides within the (a) equiaxed grained material fabricated with the point heat source fill, (b) columnar grained material fabricated with the raster scan strategy.

Mechanical Test Specimen Microstructure

Figure 6a and b shows representative as-fabricated and post-processed grain orientation maps along the build direction taken from material fabricated for the mechanical testing using both the standard raster scan and point heat source fill based on the parameters detailed in section "Mechanical Test Sample Build". Through post-processing of the two grain structures, the as-fabricated states are retained.

As a result of post-processing, the equiaxed grains within point heat source fill material did undergo grain growth as evidenced by the shift in the range of grain size from 180 μm to 240 μm range in the as-fabricated state to 270–310 μm in the post-processed state. The grain growth is attributable to the combined lack of carbides or precipitate phase along the grain boundaries to act as a Zener pinning mechanism, as depicted in Fig. 7a, and the 1200°C HIP temperature which dissolves any grain boundary δ that may have been present. Further, the grain growth behavior can be considered consistent with observations made in wrought Inconel 718 processed above the δ solvus.[13]

Separately, the columnar texture associated with the standard raster scan fill did not undergo statistically significant change in grain width as a

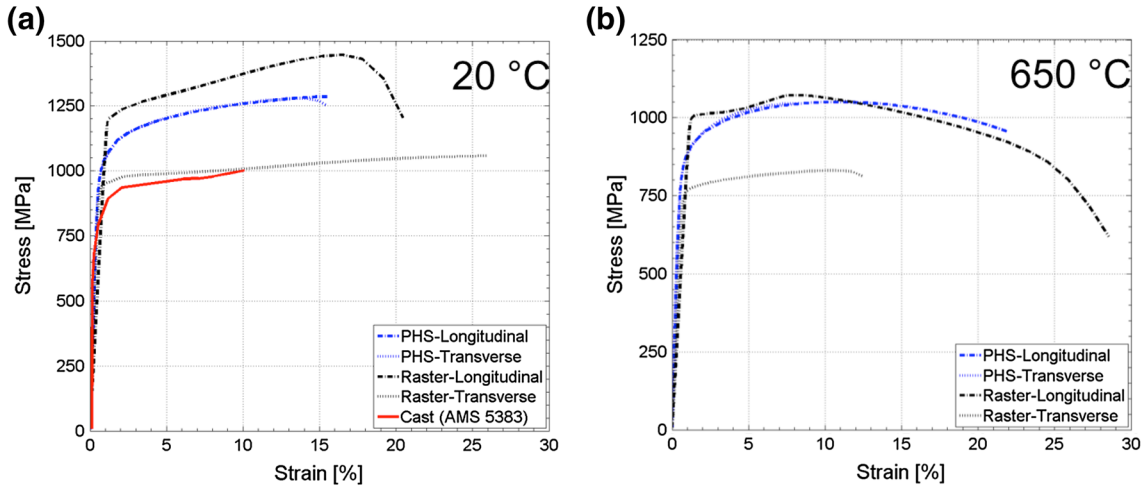

Fig. 8. Stress–strain response of EBM Inconel 718 fabricated using raster scan strategy (*Raster*) and point heat source fill (*PHS*) at (a) room temperature in relation to cast and wrought Inconel 718, (b) 650°C.

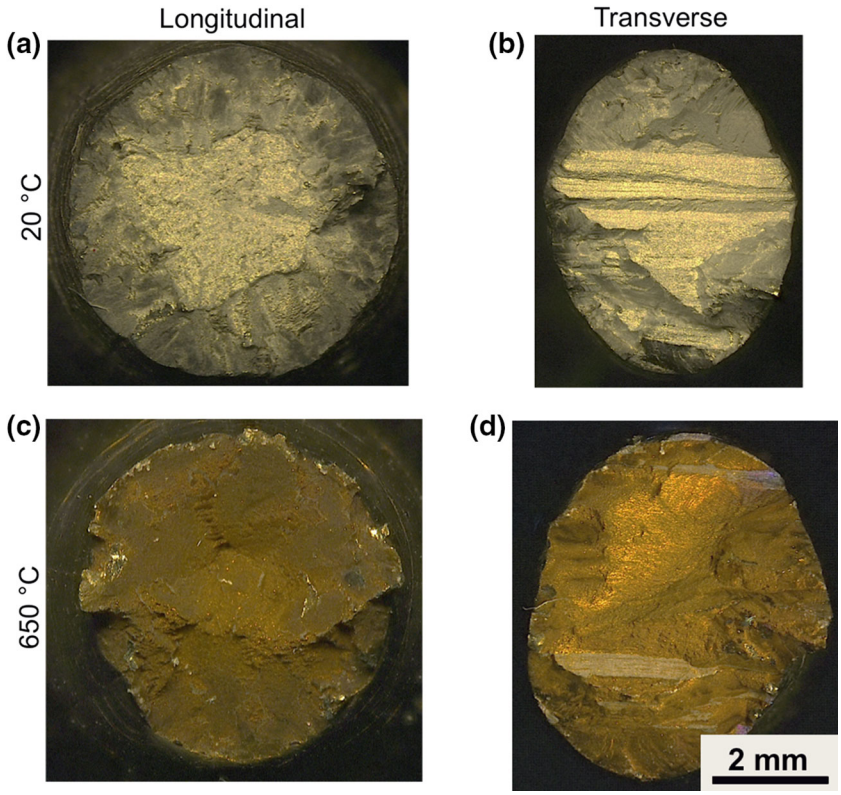

Fig. 9. Optical micrographs of the tensile fracture surfaces of the columnar-grained material fabricated using the standard raster fill within the (a) longitudinal orientation at 20°C, (b) transverse orientation at 20°C, (c) longitudinal orientation at 650°C, (d) transverse orientation at 650°C.

result of post-processing. In this instance, the grain width was measured to be in the range of 200–500 μm, with the grains having lengths spanning several mm. The lack of grain growth here can be attributed to Zener pinning provided by carbides that string the grain boundaries of the columnar grains, as shown in Fig. 7b.

Mechanical Behavior

Representative tensile stress–strain responses at room temperature and 650°C for each of the textures and orientations [longitudinal (*XZ* plane) and transverse (*XY* plane) to the build direction] are presented in Fig. 8a and b, respectively. For

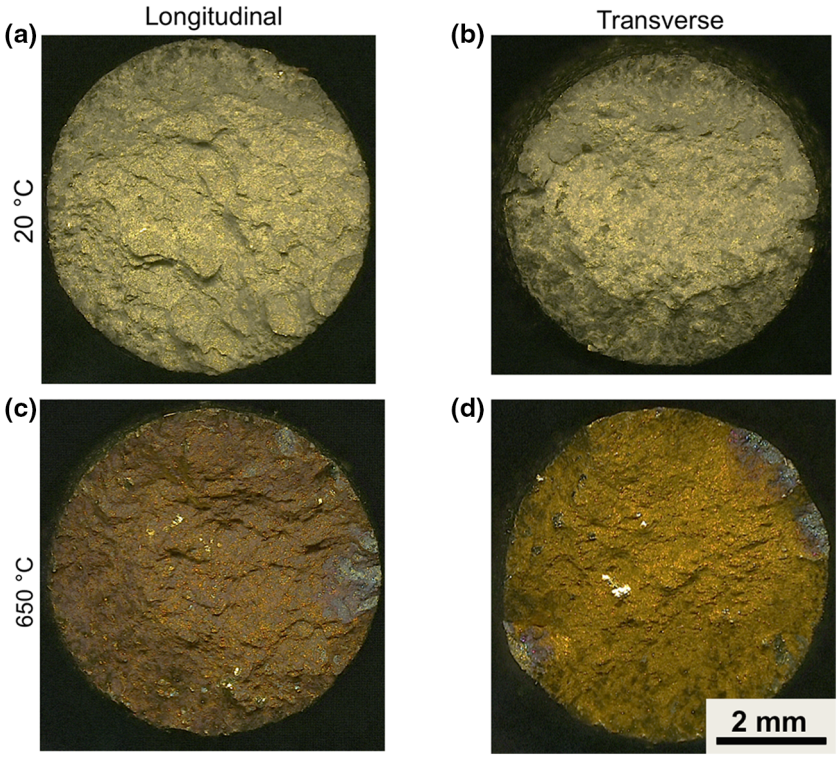

Fig. 10. Optical micrographs of the tensile fracture surfaces of the equiaxed grained material fabricated using the point heat source fill within the (a) longitudinal orientation at 20°C, (b) transverse orientation at 20°C, (c) longitudinal orientation at 650°C, (d) transverse orientation at 650°C.

reference, the standard (AMS 5383) stress–strain response of investment cast Inconel 718 is included at room temperature.[14] It should be noted that the mechanical behavior of Inconel 718 is particularly sensitive to the solution and aging time and temperatures, and the cast material is only provided as a reference.[15]

Transitioning from the longitudinal to transverse orientation in the columnar grained Inconel 718, a 30% increase in the elastic modulus is observed, with a corresponding 30% on average decrease in both the yield stress and ultimate tensile strength at room temperature and 650°C. These changes in the properties fall within the typical behavior exhibited by cast directionally solidified Ni-base superalloys when tested parallel and transverse to the solidification direction.[9,16,17] Comparatively, the two material orientations undergo linear hardening at room temperature; however, at 650°C, the longitudinal columnar-grained response exhibits the appearance of perfectly plastic or heterogeneous slip immediately after yielding, after which the material begins to gradually strain-harden under multi-slip conditions. Near-identical tensile behaviors have been reported for fine-grained Inconel 100[18] and single-crystal CMSX-2[19] in the intermediate temperature regime.

Figure 9 shows the fracture surfaces of the columnar-grained material at room temperature and 650°C. Different fracture mechanisms can be observed between the two material orientations. In the longitudinal orientation, the material undergoes intergranular failure, whereas when pulled transverse to the columnar grains, a drastic distortion of the gage section is observed. This is attributable to the rotation of the columnar grains to bring the slip planes of greatest resolved shear stress into alignment with the loading direction.[20] In the instance of Inconel 718, this would be the {111} family of slip planes.

When compared, the tensile behavior of the point heat source fill parallel to the build direction and transverse to it exhibit an isotropic stress–strain response with $<1\%$ deviation between the elastic moduli, yield stress, and ultimate tensile strength. Further, in keeping with the trend of Ni-base superalloy cast in both polycrystalline and directionally solidified forms, the equiaxed behavior predictably falls between the longitudinal and transverse behaviors of the columnar-grained material.[16,9] In addition, at room temperature, the point heat source fill material exhibits similar Young's moduli values to that of the traditionally cast and wrought materials at room temperature of 200 GPa.[21,14] Further, when compared to the room temperature yield strength of direct-aged wrought Inconel 718 as a function of grain size, good agreement is seen when the trend is extrapolated to the grain sizes observed here.[22] Figure 10 shows the representative fracture surfaces of the point heat source fill material tested at both 20°C and 650°C in both the longitudinal and transverse

orientations. Between the two orientations, identical fracture surfaces are observed unlike in the columnar-grained material.

While the post-processing conditions chosen for this study resulted in beneficial properties for both the columnar- and equiaxed-grained materials, further efforts are required in optimizing the mechanical performance of the material. In particular, to limit the grain growth that the equiaxed material experiences and promote the Hall–Petch strengthening mechanism.[22] However, providing generalized conditions for optimizing the microstructure of Inconel 718 is difficult due to the material being given customized post-processing treatments based on the specific application of the material/components.[15]

CONCLUSIONS

In this work, an alternative point heat source fill was demonstrated for controlling the texture of the Ni-base superalloy Inconel 718 in the EBM process on a bulk scale. Through changes in key parameters in the point source fill, it was shown that materials with both columnar- and equiaxed-grained structures could be obtained in the as-fabricated state. The determination of whether columnar or equiax grains form in the point heat source fill is determined by the imparted energy in the series of points, and the ability for the melt pool to merge with neighboring melt pools on successive rows. In the case of the standard raster scan, the melt pool remains localized and the columnar grains aligned with the build direction result.

Upon post-processing the material, the texture was found to remain consistent with the as-fabricated material, while grain growth was experienced due to the lack of carbides to pin the grain boundaries as in the columnar-grained material fabricated through the standard raster scan. Monotonically, the equiaxed material formed using the point heat source fill resulted in isotropic tensile properties that fell between those of the columnar-grained material when tested both parallel to the building direction and transverse to it.

ACKNOWLEDGEMENTS

This research sponsored by the US Department of Energy, Office of Energy Efficiency and Renewable Energy, Advanced Manufacturing Office, under contract DE-AC05-00OR22725 with UT-Battelle, LLC.

REFERENCES

1. I. Gibson, D.W. Rosen, and B. Stucker, *Additive Manufacturing Technologies* (New York: Springer, 2010).
2. M.M. Kirka, F. Medina, R.R. Dehoff, and A. Okello, *Mater. Sci. Eng. A* 680(5), 388 (2017).
3. M. Gäumann, S. Henry, F. Cléton, J.D. Wagnière, and W. Kurz, *Mater. Sci. Eng. A*, 271(1–2), 232 (1999).
4. S. Babu, M. Miller, J. Vitek, and S. David, *Acta Mater.*, 49(20), 4149 (2001).
5. G. Dinda, A. Dasgupta, and J. Mazumder, *Scr. Mater.* 67, 503 (2012).
6. R.R. Dehoff, M.M. Kirka, W.J. Sames, H. Bilheux, A.S. Tremsin, L.E. Lowe, and S.S Babu, *Mater. Sci. Technol.* 31(8), 931 (2015).
7. H.E. Helmer, C. Körner, and R.F. Singer, *J. Mater. Res.* 29, 1987 (2014).
8. H. Helmer, A. Bauereiß, R.F. Singer, and C. Körner, *Mater. Sci. Eng. A* 668(6), 180 (2016).
9. M. McLean, *Directionally Solidified Materials for High Temperature Service* (London: The Metals Society, 1983).
10. http://www.arcam.com/. Tech. rep (February 7, 2016).
11. *ASTM E21–09 Standard Test Methods for Elevated Temperature Tension Tests of Metallic Materials*. Tech. rep., ASTM International (2009).
12. *ASTM E08–13a Standard Test Methods for Tension Testing of Metallic Materials*. Tech. rep., ASTM International (2013).
13. A. Koul, P. Au, N. Bellinger, R. Thamburaj, W. Wallace, and J. Immarigeon, *Development of a Damage Tolerant Microstructure for Inconel 718 Turbine Disc Material*. In: Superalloys 1988, S. Reichman, D. Duhl, G. Maurer, S. Antolovich, and C. Lund, eds., pp. 3–12 (1988).
14. U. S. D. of Defense, *Metallic materials and elements for aerospace vehicle structures*. No. v. 5 in Military handbook. U.S. Dept. of Defense (1994).
15. F.R. Preli and D. Furrer, *Lessons Learned From The Development, Application And Advancement Of Alloy 718*". In: 8th International Symposium on Superalloy 718 and Derivatives, E. Ott, A. Banik, X. Liu, K. H. Ian Dempster, J. Andersson, J. Groh, T. Gabb, R. Helmink, and A. Wusatowska-Sarnek, eds., pp. 3–14 (2014).
16. R.C. Reed, *The Superalloys Fundamentals and Applications* (Cambridge: Cambridge University Press, 2006).
17. K. Harris, G. Erickson, R. Schwer, *Superalloys* 1984, 221 (1984).
18. M. Burba, D. Buchanan, M. Caton, R. John, and R. Brockman, Microstructure-sensitive model for predicting surface residual stress relaxation and redistribution in A P/517 M nickel-base superalloy. In: M. Hardy, E. Huron, U. Glatzel, B. Griffin, B. Lewis, C. Rae, V. Seetharaman, and S. Tin (eds) *Superalloys*, pp. 619–627 (2016).
19. P. Caron and T. Khan, Tensile behaviour of a nickel-based single crystal superalloy: effects of temperature and orientation. In: T. Khan and A. Lasalmonee (eds) *Advanced Materials And Processing Techniques For Structural Applications*, pp. 59–70 (1982).
20. A. Khan and S. Huang, *Continuum Theory of Plasticity* (New York: Wiley, 1995).
21. *Inconel alloy 718*. Tech. Rep. SMC-045, Special Metals Corporation (2007).
22. E.L. Raymond, Effect of chemistry and processing on the structure and mecanical properties of inconel alloy 718. In: E. Loria (ed) *Superalloy 718: Metallurgy and Applications* (Minerals, Metals & Materials Society, 1989), pp. 577–587.